Supporting Information

Ivanov and Mizuuchi 10.1073/pnas.0911036107

SI Materials and Methods

Preparation of the Proteins, Buffers, and Lipids. MinCDE genes were isolated by PCR from *E. coli* K-12 genomic DNA and cloned into pCR-Blunt II-TOPO plasmid using Zero Blunt TOPO PCR Cloning Kit (Invitrogen). The gene sequences were compared to our design and K-12 genome data after each step. The individual genes of interest were amplified by PCR and cloned into ampicillin resistant pET100/D-TOPO (MinD) or custom modified pET41/42 (MinE) expression vectors from Invitrogen pET Directional TOPO Expression Kits. For fluorescent versions, Min genes were fused to EGFP gene at the 3′ (MinD) or 5′ (MinE) ends using PCR. The termination codon of the MinE gene (not fused to EGFP) was replaced with CAC CAT CAC CAT CAC CAT TAA to add 6His-tag. The EGFP-MinD construct had a His-tag at the N-terminal (delivered from the vector) and the termination codon for the EGFP gene and the initiation codon for the MinD gene were replaced by TCT CGG to generate a Ser-Arg linker.

The protein expression plasmids were introduced into BL21-AI cells. Four liter cultures in LB broth supplemented with 100 mg l^{-1} carbenicillin were grown at 37 °C to OD_{600} = 0.5–0.6, induced with 0.2% arabinose and 1 mM IPTG, and expressed overnight at 16 °C. Cells were chilled on ice and harvested by centrifugation, frozen by liquid nitrogen, and stored at −80 °C. The cell pellets were suspended in 150 mL of lysis buffer [20 mM potassium phosphate, 0.15 M NaCl, 40 mM imidazole, 5 mM β-mercaptoethanol (BME)] with Complete Protease Inhibitor Mixture Tablets (Roche), and lysed by using a Microfluidizer (Microfluidics Corporation). The debris were cleared by centrifugation and filtration through 0.22 μm pore size membrane and loaded onto a 5 mL HisTrap HP Ni column (GE Healthcare) equilibrated with lysis buffer. The column was washed with high salt buffer (20 mM potassium phosphate, 0.9 M NaCl, 40 mM imidazole, 5 mM BME) and eluted by an imidazole gradient. The buffer of the protein containing fractions was exchanged to 25 mM hepes pH 7.5, 100 mM NaCl, 0.1 mM EDTA, 10% glycerol by gel filtration, and the sample was concentrated using an Amicon Ultra-15 30 kDa or 5 kDa (for MinE) MWCO centrifugal filter device (Millipore) to a final concentration of 3–12 mg mL^{-1}. Proteins were aliquoted, frozen, and stored at −80 °C, or kept in high glycerol buffer (25 mM hepes, pH 7.25, 0.45 M KCl, 0.1 mM EDTA, 1 mM DTT, and 50% wt/wt glycerol) without freezing at −30 °C. MinE was coupled to maleimide Alexa647 according to the manufacturer's protocol as described in ref. 1; the unreacted dye was removed by using a Sephadex G-25 column. The labeling efficiency measured with fluorometer was approximately 90%.

Protein oligomerization in the absence of lipids was tested by crosslinking with disuccinimidyl suberate (Thermo Scientific). The crosslinking was quenched with 1 M TrisCl and the products were analyzed on a NuPage Tris-Bis 4–12% gel with Mes SDS buffer. MinE was found to be a dimer, but we could not find any evidence for significant dimerization or oligomerization of MinD in the presence or absence of 2 mM ATP and 10 mM $MgCl_2$.

We used buffer A (25 mM Tris pH 7.5, 150 mM KCl) for the lipid preparation. For the in vitro self-organization assay we used the reaction buffer (buffer A plus 5 mM $MgCl_2$, 2.5 mM ATP, and 1 or 1.8 mg mL^{-1} ascorbic acid neutralized by KOH). The reaction mixture containing 1.06 μM EGFP-MinD and 1.36 μM MinE-Alexa647 was incubated for 15 min at 37 °C before loading into the flow cell. The experiments were performed at room temperature of 22–23 °C unless otherwise noted.

All lipids were purchased as chloroform solution from Anvanti Polar Lipids. We used three types of lipid mixtures for bilayer preparation, natural *E. coli* polar lipids (*E. coli* lipid bilayer), synthetic monounsaturated lipid mix (18:1 bilayer), and synthetic 70% double-unsaturated lipid mix (18:2 bilayer). The synthetic 70% double-unsaturated lipid mix contained 70% (by mass) 18:2 PE (1,2-dilinoleoyl-*sn*-glycero-3-phosphoethanolamine), 25% DOPG [1,2-dioleoyl-*sn*-glycero-3-phospho-(1'-*rac*-glycerol) (sodium salt)], and 5% CL [1,1'2,2'-tetraoleoyl cardiolipin (sodium salt)]. The synthetic monounsaturated lipid mix contained 70% DOPE (1,2-dioleoyl-*sn*-glycero-3-phosphoethanolamine), 25% DOPG, and 5% CL. We used *E. coli* lipid bilayer for most of the experiments for observation of the oscillation, waves, some snakes, and immobile amoeba related structures. For observation of the dynamic amoebas and their development from oscillation or waves we typically used 18:2 bilayer. For observation of snakes and dynamic amoebas at elevated temperature (approximately 25 °C) we used 18:1 bilayer.

The 2.5% lipid mixtures in 0.2 mL of chloroform were dried onto the borosilicate glass tube wall with a nitrogen stream. The tube was dried for 3 h in a Speedvac (Savant) and hydrated with buffer A overnight at 4 °C without shaking. The tube was vortexed and sonicated in a cup horn sonicator (Misonix) with water circulation at room temperature until the small unilamellar vesicle (SUV) solution become clear (approximately 65 W for 15 min). The resulting SUV suspension was stored under Nitrogen at 4 °C for up to 10 days (3 days for suspensions containing double-unsaturated lipids). Before loading into the flow cell the SUV suspension was diluted five times with buffer A and warmed to room temperature; 5 mM $MgCl_2$ (3 mM $MgCl_2$ for solutions containing double-unsaturated lipids) was added just before loading into the flow cell. The flow cell was slowly loaded with SUV suspension and incubated at room temperature for approximately 1 h, and was washed with buffer A with 5 mM $MgCl_2$ before the experiment. The lipid membrane surface used for the experiment was flat both before and after exposure to Min proteins, according to AFM scans in a wet mode (with ATP–protein mix loaded mica-supported lipid bilayer); no localized large deformation of lipid membrane was detected.

Flow Cell. The flow cells were assembled on fused silica slides with drilled holes (Esco Products). The slides were washed with Hellmanex II soap (Hellma), rinsed extensively with deionized water, and air dried for at least 2 h. A 4-mm-wide flow channel was cut on a piece of 25-μm-thick acrylic transfer tape (3M) and placed between a cover glass and the fused silica slide. The 25-μm thickness of the flow cell was verified by focusing a microscope on the top and the bottom flow cell surfaces. Nanoport N-333–01 inlets (Upchurch) were attached to the fused silica slides above the holes using Optical Adhesive 61 (Norland Products). Each flow cell had one or two inlets and one outlet (separated 3 cm from the inlet). The inlets were connected to sample syringes with 0.02-in inner diameter tubing.

The reaction solution containing proteins was loaded to the syringe and the tubing before connection to the flow cell. For most of the experiments the constant sample pumping rate was maintained at 3 μL min^{-1}, which corresponds to a cross-section average flow velocity inside the flow cell of 0.5 mm s^{-1}. The pumping compensates any depletion of the proteins near propagating wave with average flow velocity three orders of magnitude faster than the typical wave-front velocity, and Taylor dispersion (2) across laminar flow profile is estimated to take place on the time scale of about two orders of magnitude faster than the typical wave periods.

The buffer flow change generally did not have a noticeable large effect on the observed system behavior at steady states, indicating

that the dynamic pattern formation is not significantly dependent on the reaction component concentration inhomogeneity in the solution immediately above the membrane surface, which might arise during the reaction under certain experimental conditions. However, at the beginning of the reaction, the sample loading procedure and the distance of the observation location from the sample inlet made a significant impact as discussed in *Supporting Data*.

Microscope, Camera, and Illumination. For all our experiments we used a total internal reflection fluorescence (TIRF) microscope setup with the prism installed over an inverted Eclipse TE2000E microscope (Nikon) with Plan Apo VC 100× NA = 1.40 oil-immersed objective and magnifier setting 1×. The illumination laser lines were blocked between the objective and camera with LineStop filters (Semrock) for the corresponding wavelengths. All images and movies were acquired using an Andor DU-897E camera (Andor Technology) with integrated shutter, through a DualView (Photometrics) with dcxr630 insert, which provides separation at 630 nm for two color acquisition. The spatial resolution of the camera images were 6 pixels per micrometer with a 512 × 512 pixels viewing area. The typical setting for the camera were digitizer 1MHz (16-bit gray scale), preamplifier gain 5.2, vertical shift speed 2MHz, vertical clock range: normal, EM gain 80, EM CCD temperature set −100 °C, baseline clamp ON, exposure time 100 ms, frame rate 0.5 or 0.33 Hz. The intensity data for the other regimes were renormalized for the above settings and the baseline of approximately 100 camera units subtracted from the data.

The illumination for EGFP and Alexa647 labeled molecules was provided by 488 nm DPSS (Sapphire, Coherent) and 633 nm HeNe (Research Electro-Optics) lasers correspondingly. Laser power was adjusted with 60 dB range calibrated and computer controlled power attenuators (OZ Optics). The beams were fiber coupled into single mode and polarization maintaining optical fibers The different colors were combined into a single fiber by a combiner with shutter and delivered to the output collimator. The illumination beam shutter was closed between frames. The s-polarized evanescent wave was created using a 70° fused silica dove prism. The power of the 488 nm laser was calibrated and the intensity data for different laser power levels were normalized on the graphs according to the power setting and camera settings. The illumination had a Gaussian shape in the field of view with a measured horizontal and vertical half maximum widths of 65 × 172 μm at 488 nm. The intensity data for the graphs were taken from the middle of the illumination profile. The illumination profile in the movies was not flattened. The typical intensity of the 488 nm illumination center at the flow cell surface was approximately 0.05 W cm^{-2} (estimated from the measured beam power and intensity profile).

Metamorph 7 software (Molecular Devices) was used for camera control and image acquisition and analysis. The brightness and contrast range were set for each picture or movie individually for the best representation of the features of interest. As a result some darker or brighter features present might not be clearly visible. The more precise intensity data can be extracted from the graphs of intensity time-course measured at fixed locations. The graphs were scaled, if required, to the standard illumination conditions and camera settings, for which 1 camera unit (c.u.) corresponds to a molecular surface density of approximately 1.8 μm^{-2} as described below. ImageJ software (National Institutes of Health) was used for final conversion of Metamorph movies into QuickTime. Movies are accelerated 60 times.

Wave velocities were directly measured from Movie S1 and other movies using Metamorph software by monitoring the motion of the wavefront at 50% of the peak level. Wavefront velocity varied somewhat between experiments, but in each experiment, the velocity of the waves was roughly a half of the velocity of the expansion of the initial circular binding zones in the preceding oscillation, regardless of the exact wave velocity.

Estimation of the Protein Surface Concentrations. The measured fluorescence intensity signal was proportional to the volume concentration of fluorescent molecules multiplied by the penetration depth of the evanescent wave (128 nm for 488 nm beam) plus the surface concentration of fluorescent molecules. The volume contribution to the fluorescence intensity signal was much smaller compared to the contribution of the surface for our EGFP-MinD and Alexa647-MinE mixtures at the concentration range used, except during the binding time lag before initial binding of proteins in the middle of the flow cell. The surface density of EGFP-MinD was estimated by comparison between the fluorescent signals from EGFP-MinD and ParA-GFP samples. ParA-GFP has no affinity to the lipid bilayer (verified by buffer exchange). The spectrum of ParA-GFP is similar to EGFP-MinD, but the ParA-GFP brightness is 1.6× lower (verified by bulk fluorometer measurements). We estimated that a typical peak intensity level in the EGFP-MinD channel of 7,000 c.u. corresponds to a coverage density approximately 1.25×10^4 μm^{-2} or 80 nm^2 per molecule, which is two to three orders of magnitude less than used in the theoretical modeling in ref. 1. Thus we conclude that bulk volume depletion due to surface binding is insignificant in the presence of the buffer flow and the constant and homogeneous total volume concentration of proteins during the reaction is a good approximation for experiments reported here.

The Alexa647-MinE channel was not directly calibrated, but the surface density of the Alexa647 labeled MinE molecules was estimated from the experiments with EGFP-MinE fusion protein. EGFP-MinE fluorescence intensity was measured in oscillation and wave regimes over *E. coli* lipid bilayer with nonfluorescent MinD. The peak surface density of MinE-EGFP was two to four times less (2.6 times is our best estimate, which was used for normalization of Alexa647-MinE intensity data) than the peak surface density of EGFP-MinD measured in the experiments with the same type of self-organization behavior and the same laser power and camera settings. In the experiments with MinE-Alexa647 the surface concentration of MinE was assumed to be the same as that for the same type of dynamic behavior with MinE-EGFP.

Our surface density estimate of MinD and MinE did not significantly change when the fluorescence-labeled proteins were diluted by nonlabeled proteins. We also have not noticed any significant bleaching of the fluorophores by TIRF illumination even at increased illumination levels used for experiments with 1% fluorescently labeled and 99% unlabeled proteins. Comparison of the intensity data between the experiment with 1% fluorescently labeled and 99% unlabeled proteins and the experiment with 100% fluorescently labeled proteins did not reveal any significant autoquenching of fluorophores. Channel crosstalk and FRET between EGFP and Alexa647 were detected, but the levels were small and did not significantly influence (less than few percent in most cases) our measurements. Therefore, the images for the two channels were not corrected for these effects.

FRAP Experiments. For the FRAP experiments we used parallel beam illumination with an approximately 50 mW beam from a 488 nm DPSS laser converted to circular polarization by a quarter-wave plate introduced through the back port. The laser beam was defocused using a −50 cm planoconcave lens placed in the filter cube in place of excitation filter. The beam was reflected into the objective by a 45° 488 nm RazorEdge dichroic mirror (LPD01-488RS, Semrock). The beam was controlled by a shutter. The resulting 12-μm diameter round circle with near uniform intensity and sharp edges could be bleached upon 2 s exposure at maximal power. The power of the laser was sufficient for bleaching not only EGFP but also Alexa647 to a lesser degree. If the FRAP experiment was performed in the absence of ascorbic acid or oxygen scavenger, we observed a frozen circular area, which was darker than the wave peak, but brighter compared to wave minima. We interpret these effects to be caused by light activation of free

radicals that leads to crosslinking between molecules (3). The crosslinking effect was noticeable even when only a few percent of the molecules were bleached. Photocrosslinking could take place over the evanescent illumination area if very strong illumination was used for image acquisition even without a FRAP experiment. To avoid photocrosslinking the FRAP experiments were performed in the presence of ascorbic acid at a concentration of 1–2 mg ml^{-1}. We used ascorbic acid for most measurements. We also tested an oxygen scavenger system and found no significant advantage over the use of ascorbic acid alone.

The major effect detected by FRAP was the exchange of fluorescent molecules between solution and the lipid surface. It was difficult to detect any 2D diffusion in the experiments with rapidly changing surface concentration of fluorescently labeled molecules. Inhomogeneity of residual photocrosslinking effects (the crosslinking increases with increase of the light exposure and degree of polymerization) might also make a false impression of 2D diffusion. In all FRAP experiments with fluorescently labeled proteins, except for the case of the large steady amoeba-like structure (Fig. S7*B*), we saw no evidence for a significant 2D diffusion. The nonuniform recovery observed in the case of the steady wave could be interpreted either as a biased 2D diffusion or different protein exchange dynamics at different parts of the observation area.

Supporting Data

Protein Labeling Does Not Significantly Change Its Activity for the Dynamic Pattern Formation. To evaluate the difference between the EGFP and Alexa647-tagged and unmodified MinD and MinE, the fluorescence labeled proteins were diluted 100 times with unmodified proteins. The only difference in the behavior between 100% fluorescence labeled proteins and the mixture with 1% fluorescence labeled proteins was about a twofold shorter period of waves (90-s period, 0.77-μm s^{-1} wave velocity, and 70-μm wavelength) over *E. coli* lipid bilayer. The other set of experiments were performed with fluorescent MinD and nonfluorescent MinE and vice versa and no major difference in self-organized behaviors (including period, wave velocity, and amplitude) were detected.

Summary of the Fluorescence Recovery Time Data. We calculate most of the fluorescence recovery times using single exponential fitting, which worked well for all motionless or slowly moving structures analyzed. Below we use the exponential time constants and the extent of fluorescence recovery as characteristics of the FRAP measurements. During photobleaching experiments with the large steady amoeba-like structures (Fig. S7) MinD and MinE fluorescence recovery was approximately 100% with time constants 6 s and 14 s, respectively. MinD and MinE time constants were 3.5–6.2 s and 16–20 s for fast moving amoebas, 6.3 s and 35.5 s for slow moving amoebas, and 13 s and 168 s for the frozen mesh, as in Fig. 3 *C* and *D*. We could not estimate the extent of fluorescence recovery for the slow and fast moving amoebas, because bleached amoebas tended to shrink and disappear after partial recovery. This could be due to the residual protein crosslink even in the presence of ascorbic acid. Thus the time constants for these structures are rough estimates. The recovery for frozen mesh was approximately 75% for MinD and approximately 100% for MinE.

FRAP data in the oscillation and wave experiments were analyzed by subtraction of the signal of the bleached area from the signal of a nearby unbleached area with similar amplitude and cycle phase (Fig. S10). We estimate that approximately 85% of MinD fluorescence was recovered. The time constant was in the range 7.3–20 s (depends on the time-range used for fitting, with a longer time-range leading to slower estimates) if fluorescence recovery was fitted with a single exponent. MinD fluorescence recovery can be also fitted to double exponents with time constants 3.5 s and 32 s with relative contributions of 71% and 29%. The contribution of the faster exponent might be larger in reality, because the frame rate was only 0.5 Hz. We did not detect significant fluorescence recovery for MinE during FRAP experiments with oscillation and waves, which is consistent with our hypothesis of MinE polymerization. The FRAP experiment with 100× diluted fluorophores showed a 10.7 s recovery time for MinD and no detectable recovery for MinE.

FRAP Experiments in the Absence of Ascorbic Acid or Oxygen Scavenger. Photobleaching in the absence of ascorbic acid or oxygen scavenger leads to crosslinking of the protein molecules by free radicals and generated a protein coated area that prevented progression of subsequent waves. If the circular spot was bleached near the trailing edge of a wave (Fig. S11*A*, first two frames) the subsequent wave was repelled by the bleached area (Fig. S11*A*, last three frames). Photobleaching of the circular spot near the front edge of a wave does not lead to dramatic repulsion of the front edge of the subsequent wave from the bleached spot. The wavefront of the subsequent wave is relatively straight (Fig. S11*B*). The crosslinked area gradually dissolves away after passage of many waves around it.

Our interpretation of this experiment is based on crosslinking of proteins and/or lipids under high intensity light exposure (4). As the result proteins remain frozen on the membrane in the form of initiation (for the wavefront) or dissociation (for the trailing edge) complexes, which interact with subsequent waves.

Domain Structures in the Supported Lipid Bilayer. The lipid domain structure of *E. coli* and 18:2 bilayers was visualized using 10-N-Nonyl acridine orange (NAO). The NAO was dissolved in chloroform at concentrations 2 or 0.2 mg ml^{-1} and mixed with lipids in the chloroform phase. The final concentration of NAO ranged from 2 to 0.4% with respect to the mass of lipids (the actual NAO concentrations used for different images in Fig. S1 and Movie S9 are given in the captions). NAO was excited using 488 nm laser and imaged in the "green channel" of DualView as described above (*SI Microscope, Camera, and Illumination*).

We found that the shape of cardiolipin-rich domains of *E. coli* lipid bilayer preferentially stained by NAO (Fig. S1*B*) has some similarity with the shape and spatial distribution of frozen amoebas (Fig. 3 *C* and *D*). The similar domain structure was also observed with *E. coli* lipid bilayers with added 0.1% (by mass) rhodamine B labeled DOPE [1,2-dioleoyl-*sn*-glycero-3-phosphoethanolamine-N-(lissamine rhodamine B sulfonyl), Avanti product # 810150], but we could not observe any domains by DiI (1,1′-dioctadecyl-3,3,3′,3′-tetramethylindocarbocyanine perchlorate from Invitrogen) staining. The observed surface brightness of DiI was uniform if lipids were stained although in the chloroform phase. If the vesicles were stained during sonication we observed sharp borders between large (≥50 μm) uniformly dark and uniformly bright areas without any sign of diffusion after more than one hour incubation time. We suspect that DiI dye might reduce the fluidity of solid surface-supported lipid bilayers and should be used with caution.

The FRAP experiment (Movie S9) with NAO revealed that, despite the shape of the domains changing only very slowly with time, the fluorophore diffusion is fast (diffusion coefficient 5.7 μm^2 s^{-1}) and the *E. coli* lipid bilayer is in liquid phase. We observed that after fluorescence recovery some cardiolipin-rich lipid domains started to shrink and disappear (presumably due to photodamage of the lipid) in a way similar to disappearance of amoebas after FRAP experiments (*SI Summary of the Fluorescence Recovery Time Data*). We propose that the scale of static lipid domains and the scale of dynamic amoebas might be controlled by a similar membrane stress-related mechanism.

The colocalization experiment with NAO stained 18:2 and *E. coli* lipid bilayers and Alexa647-MinE revealed no direct matches between the lipid domain shapes and dynamic structures formed by protein self-organization (nonfrozen protein patterns), but

areas with higher levels of the background proteins coincided with cardiolipin-rich domains (see yellow patterns on the right panels in Fig. S1 *C* and *D*). Dynamic amoebas developed more readily within these areas on the 18:2 bilayer.

Membrane Binding Properties of MinD in the Absence of MinE. The major fraction of the surface bound MinD is in rapid exchange with solution according to FRAP experiments. The fluorescence recovery of MinD bound to low melting temperature bilayers could be described by double exponents with time constants in the range of 4–7 and 33–140 s if the MinD was loaded in the flow cell slowly with stepwise concentration increase. The contribution ratio of the faster exponent to the slower exponent to unrecovered fluorescence in this experiment was roughly 2:1:1. If 0.0625 μM MinD was loaded into the flow cell in one step the fluorescence recovery time could be described by a single exponent with a time constant in the range of 68 s (fluorescence recovery was approximately 23%), or 19 s when the MinD concentration was 2 μM (approximately 50% recovery). The differences between the two experiments may reflect the time it took for sample loading before the FRAP experiments rather than (or in addition to) the protein concentration difference (see below). MinD binding steps during experiments with an incremental concentration increase can be described by single exponents at all concentrations ≥0.125 μM, although we have not examined extended time courses. After several loading and washing cycles the maximal binding capacity of MinD decreased 40% and the residual level of MinD that did not dissociate after each washing step (with ATP and Mg^{2+}) increased from approximately 5–50% of the maximal level. The surface binding capacity was approximately 25% less if 1 μM of MinD was loaded into the flow cell with stepwise concentration increase compared to when 1 μM MinD was loaded in one step. The observed effects could be explained by slow polymerization of MinD even in the absence of MinE. The polymerization of MinD on the membrane surface might decrease total MinD binding capacity of the lipid membrane surface and generate stable membrane bound state.

Fig. S2*A* describing MinD binding capacity was constructed from two sets of measurements: one with consecutive loading of $^1/_{16}$, $^1/_8$, $^1/_4$, $^1/_2$, $^3/_4$, and 1 μM of MinD and another with consecutive loading of 1, $1^1/_2$, 2, and 3 μM of MinD into the second flow cell. The signal for 1 μM of MinD in the second experiment was approximately 25% higher than the signal for the same concentration of MinD in the first experiment. We observed a decrease of the MinD binding capacity to the lipid membrane after several MinD loading and washing cycles as mentioned above. In Fig. S2*A* we reduced all signal levels for the second set of measurements by 20% to adjust for the signal difference in the two sets. Because of the time-dependent changes of the binding properties of the protein on the surface, the data presented in Fig. S2*A* should not be considered as simple steady state measurements.

MinD bound to the *E. coli* lipid bilayer in the presence of ATP dissociated upon buffer (with ATP and Mg^{2+}) wash with complex kinetics (Fig. S2*B*). Loosely bound MinD detached from the surface quickly during washing. The tightly bound MinD detached from the surface after a time lag, the duration of which depended on the flow cell history. The time lag was usually very short during the first loading-washing cycle, but it increased significantly after several cycles, suggesting again a time-dependent conformational change of MinD bound to the lipid bilayer or other changes that influence accumulation of a fraction of stably bound MinD that resists washing. We also observed multiple-step dissociation behavior with a low melting temperature bilayer, but the difference between the loose and tight fractions was much less pronounced (Fig. S2*C*).

Start of the Oscillation: Observation Position Effect. The observed self-organized behavior at the start of the experiment depended on the position of the observation area within the flow cell. The time lag before the first binding of MinD observed in the middle of the flow cell (Fig. S3) cannot be explained by depletion of the bulk MinD upstream of the observation spot, because the sample flow rate is large enough to compensate for bulk depletion within a time frame that is significantly shorter than the time lag. However, depletion is possible if the membrane binding competent species of the protein is a minor constituent of the bulk protein to start with. Consistent with this interpretation, the initial time lag was not detected if the observation area was located near the flow cell inlet (Fig. S3*B*) where MinD/E binding to the surface took place in the form of one period of oscillation, followed by a few periods of waves propagating in the buffer flow direction with a higher velocity and double period compared to the standard waves in the middle of the flow cell. These fast waves with a double period could be considered as an intermediate form between oscillation and normal waves: like oscillations, they have a long period and high velocity of the wave front, but they are propagating waves with a clear leading and trailing edges and the amplitude similar to that of the standard waves. After several periods, the wave propagation direction near inlet gradually became perpendicular to the buffer flow, moving from the center toward the edges of the flow, and the frequency doubled, whereas the wave directions in the middle of the flow cell away from the inlet were anisotropic with respect to the flow direction. The frequency of the near-inlet waves propagating in the direction parallel to the buffer flow remained long. Waves with different periods can coexist in the flow cell simultaneously in the spatially separated domains. Frequency of waves across the domain border is usually different by a factor of two, like in the extreme case described on Fig. 1*C*.

We conclude that certain protein species (initiation precursor) is essential for the initiation of MinD/E binding and it represents a very small fraction of the protein in the solution pumped into the flow cell. Just after the reaction mixture enters the flow cell and the proteins start interacting with the lipid surface, the preexisting initiation precursor is depleted from the solution near the inlet. During the first oscillation cycle near the inlet, a larger quantity of the initiation precursor is generated and flows down to the middle of the flow cell, which triggers MinD binding in the middle of the flow cell in the form of many circular expanding binding zones. The waves upstream provide a sufficient concentration of the initiation precursor for sustained oscillation and wave cycles down stream. The relative deficit of initiation precursor in the vicinity of the inlet causes an anisotropic wave propagation orientation. These are the only effects of the bulk solution concentration inhomogeneity dynamically generated by Min protein self-organization behavior in the presence of flow we noticed in our experiments.

The State with a High Level of the Surface-Bound MinE. We observed big differences in the self-organization behavior in the *E. coli* polar lipid coated flow cells loaded with standard reaction mixture when the sample loading method was modified. Normally, the syringe and the tubing (which were not coated with lipid bilayer) connecting to the flow cell were filled with the sample solution before connection to the flow cell, which had been coated with lipid bilayer and rinsed with buffer without Min proteins. Thus, when the sample flow was started, the lipid bilayer surface quickly encountered the preassembled sample solution. In some experiments, the standard sample solution was loaded to the flow cell through a 3-in-long piece of tubing, which was originally filled with the buffer without proteins. In these experiments, the protein concentration in the flow cell increased gradually over several minutes to the final level because of the Taylor dispersion (2). MinD and MinE binding to the surface started very slowly at the beginning, but the subsequent peak of the MinD binding rate was about twice as high as that observed with the standard method, and the surface MinE also increased rapidly to a maximum approximately3 times higher than that observed in the wave regime (compare the first binding period with the binding periods in the wave cycles later in Fig. S5). The

surface concentration of MinE did not decline sharply after reaching the maxima, but was followed by a plateau after approximately 1,400 s in the experiment shown. The MinD peak surface density was close to the surface density for oscillation. The beginning of MinD detachment was also similar to oscillation, but as the MinE plateaued, the MinD level also plateaued at approximately 50% of the peak level for the usual waves. It was possible to escape from the high steady surface level of MinD and MinE by increasing the pumping rate several times (stepwise increase to 6 μL s^{-1} at 1,510 s, to 12 μL s^{-1} at 1,961 s, to the final velocity of 20 μL s^{-1} at 3,030 s) and then decreasing the pumping rate to the normal level (at 3,357 s). Based on the MinE surface density and MinD/MinE ratio curves (Fig. S5) we suggest that during gradual bulk protein concentration increase, a much higher than normal amount of the initiation precursor accumulated and bound to the surface. This somehow resulted in very high surface density of the initiation complex and overpolymerization of MinE, which apparently failed to trigger fast dissociation phase, trapping the system in an abnormal steady state, until the faster solution flow caused a decrease of the initiation precursor concentration. A similar state with a high level of surface bound MinE was observed in an experiment with 40% lower MinE concentration (0.82 μM instead of 1.36 μM MinE) with the standard pumping protocol. We suggest that a lower volume concentration of MinE leads to an initially higher degree of surface MinD polymerization and eventually a higher surface density of MinE that associates with the MinD polymers. Certain combinations of sample loading steps appear to generate unusually high concentrations of the initiation precursor in the solution, combined with high surface density of MinD–MinE copolymers and trap the system in a (meta)stable steady state with higher than normal surface MinE density. Presumably, this situation does not materialize inside normal bacterial cells because of the high surface area to volume ratio with limiting total protein concentrations.

Labyrinth on *E. coli* Lipid Bilayer. Observation of dynamic amoebas appears to depend on the lipid bilayer fluidity. Less fluidic lipid bilayers, such as *E. coli* lipid bilayers or 18:1 bilayers at room temperature did not support dynamic amoebas. However, we observed formation of amoeba-related structures on *E. coli* and 18:1 lipid bilayers. The most commonly observed such structures were labyrinths, a fine mesh structure composed of MinD and MinE, which had some similarity to E-rings and E-mesh (labyrinth lines typically are finer than E-rings) but lacking the MinD core (Fig. S8*C*). Once formed the structure is frozen in its shape, but the components are in flux. When the labyrinth is composed of relatively thin lines of the proteins, propagating waves could pass over it without obvious impedance, and in many instances the labyrinth is almost completely erased by the passing wave, only to reappear behind the wave (Movie S1). When it reappears, the new labyrinth pattern is superimposable with the original pattern, indicating a spatial memory. When the labyrinth develops to have robust bright lines of the protein components, the lines block progression of the on-coming waves. A wave may find a passable opening in the pattern and spread into a compartment, only to find itself trapped and dissipate (Movie S3).

We believe that the frozen labyrinth is composed of the same material as the E-rings of amoebas trapped at the fault lines of the lipid bilayer. The fault lines might be the boundaries between membrane domains of the same lipid composition but with different tilt directions of the aliphatic tails. Some of the patterns reported with protein-free lipid membranes and other 2D films closely resemble our labyrinth (4, 5). We do not know whether the pattern preexisted before protein arrival or if it was generated as the labyrinth developed for the first time and then became fixed in the bilayer structure. Either way, this interpretation of the observation indicates that the E-ring-like assembly on the membrane has high affinity to the membrane structure fault lines, and this explains the memory effect mentioned above. We have not examined the membrane fluidity in the same experiments in which labyrinth has been observed to evaluate if the membrane needs to be in the gel state for the labyrinth to develop.

Giant Amoeba on *E. coli* Lipid Bilayer. Another amoeba-related structure observed on *E. coli* lipid bilayers was a giant motionless amoeba with a large D-core surrounded by a background area with less densely bound proteins (Fig. S7*A*). It was bordered by a stationary straight and thin E-line on one side, which we believe marks an underlying lipid fault line stretched in the flow direction and a broad and less pronounced E-ring on the surrounding border elsewhere. Except for small fluctuations of the E-ring shape, the area did not move, but the protein components exchanged quickly according to FRAP; the approximate fluorescence recovery time was 6 s for MinD (Fig. S7*C*) and 14 s for MinE. This giant amoeba developed from a remnant of a propagating wave stuck near the fault line, after other propagating waves disappeared. We suggest this type of rare pattern develops when the density of the dissociation centers in the surrounding area becomes high and it counter acted the wave propagation, resulting in the formation of the E-ring although the E-line behind became a constitutive wave initiation site, thus preventing the transition to the standard amoeba-like structures or the labyrinth.

Step-Like Wave Propagation. Not all anomalies in propagating waves develop into amoebas. On some occasions, waves on *E. coli* lipid bilayers propagated in a step-like fashion but did not convert into compact amoeba-like structures (Fig. S8*A*). Propagation sometimes paused without the standard amoeba development and the waves later developed multiple protrusions from the stalled front, which merged to form a next "step" (Fig. S8*B*). MinE was not labeled in this experiment.

1. Loose M, Fischer-Friedrich E, Ries J, Kruse K, Schwille P (2008) Spatial regulators for bacterial cell division self-organize into surface waves in vitro. *Science* 320:789–792.
2. Taylor GI (1953) Dispersion of soluble matter in solvent flowing slowly through a tube. *Proc Roy Soc A* 219:186–203.
3. Ayuyan AG, Cohen FS (2006) Lipid peroxides promote large rafts: Effects of excitation of probes in fluorescence microscopy and electrochemical reactions during vesicle formation. *Biophys J* 91:2172–2183.
4. Fischer TM, Bruinsma RF, Knobler CM (1994) Textures of surfactant monolayers. *Phys Rev E Stat Phys Plasmas Fluids Relat Interdiscip Topics* 50:413–428.
5. Seul M, Andelman D (1995) Domain shapes and patterns: The phenomenology of modulated phases. *Science* 267:476–483.

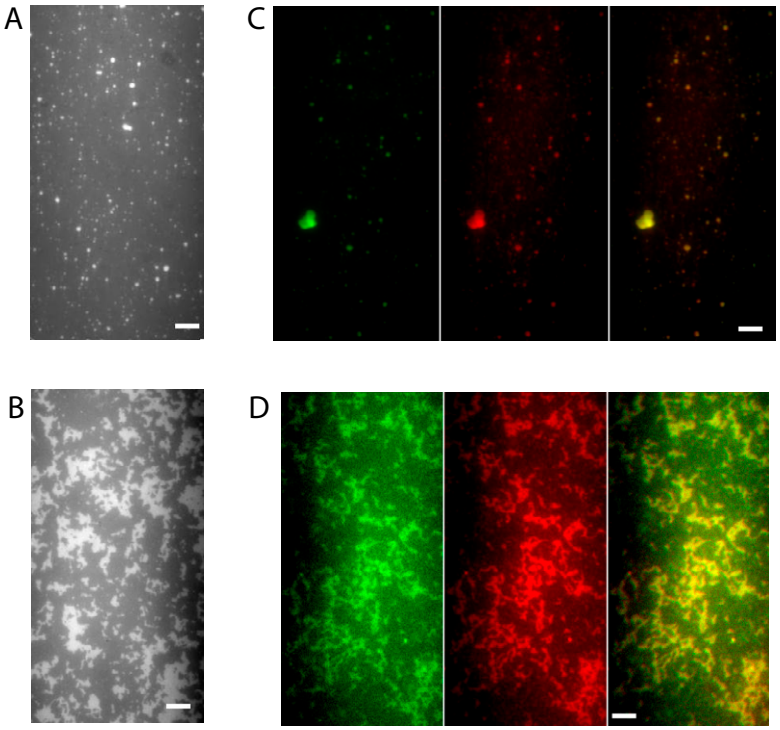

Fig. S1. Cardiolipin-rich lipid domains visualized with NAO excited by 488 nm laser beam. The brightness level is differently adjusted for different pictures. (Scale bars: 5 μm on all figures.) The flow direction is from the left to the right. (*A*) 18:2 bilayer with 2% (with respect to mass of the lipids) NAO, typical distribution. (*B*) *E. coli* lipid bilayer with 2% NAO. Some areas have no or very little of brighter domain structures. (*C*) Colocalization (*Right*) of 0.4% NAO (green, *Left*) and Alexa647-MinE (red, *Center*) averaged in the interval between waves on 18:2 bilayer. The largest spot is not typical. (*D*) Colocalization (*Right*) of 2% NAO (green, *Left*) and Alexa647-MinE (red, *Center*) averaged in the interval between waves over *E. coli* lipid bilayer.

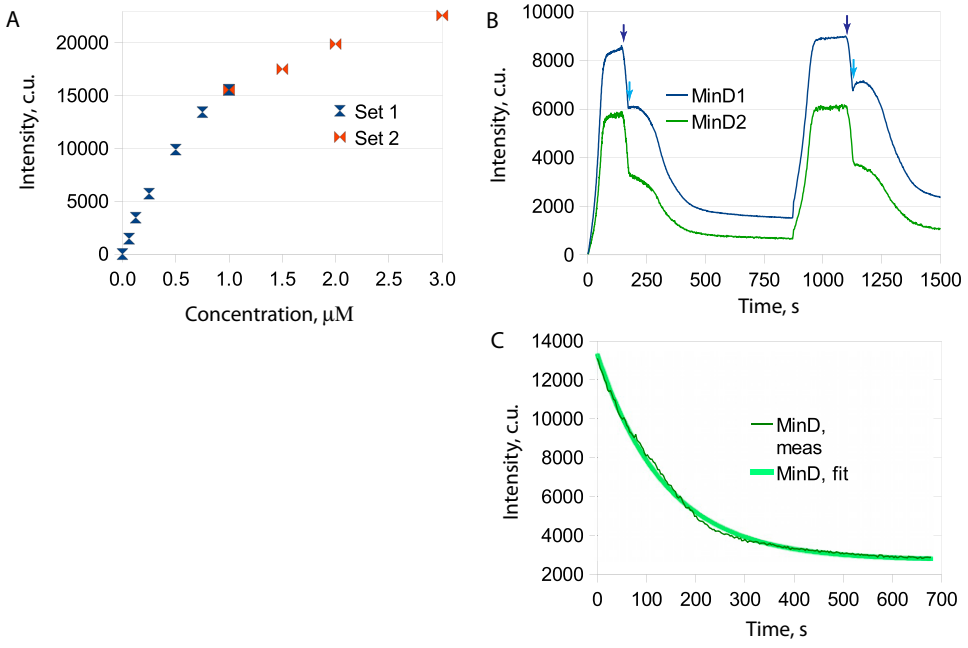

Fig. S2. MinD surface binding in the absence of MinE. (*A*) Concentration dependence of MinD surface density on the 18:2 bilayer measured in camera units (c.u.). Two data sets used in this graph are described in *SI Membrane Binding Properties of MinD in the Absence of MinE*. On all graphs 1 c.u. intensity level corresponds to a surface density of the molecules of approximately 1.8 μm^{-2} (*SI Estimation of the Protein Surface Concentrations*). (*B*) Time-course of MinD surface binding in the absence of MinE during two cycles of MinD (0.84 μM with ATP) loading and buffer (with ATP) washing on *E. coli* lipid bilayer measured at two different surface spots revealed MinD binding level as well as two steps in MinD dissociation. Beginnings of the first and second dissociation steps are labeled with dark and bright blue arrows correspondingly. (*C*) MinD (1 μM with ATP, 18:2 bilayer) washing with buffer (with ATP) revealed complex dissociation kinetics. Single exponential fit with time constant 137.8 s is overlaid for comparison.

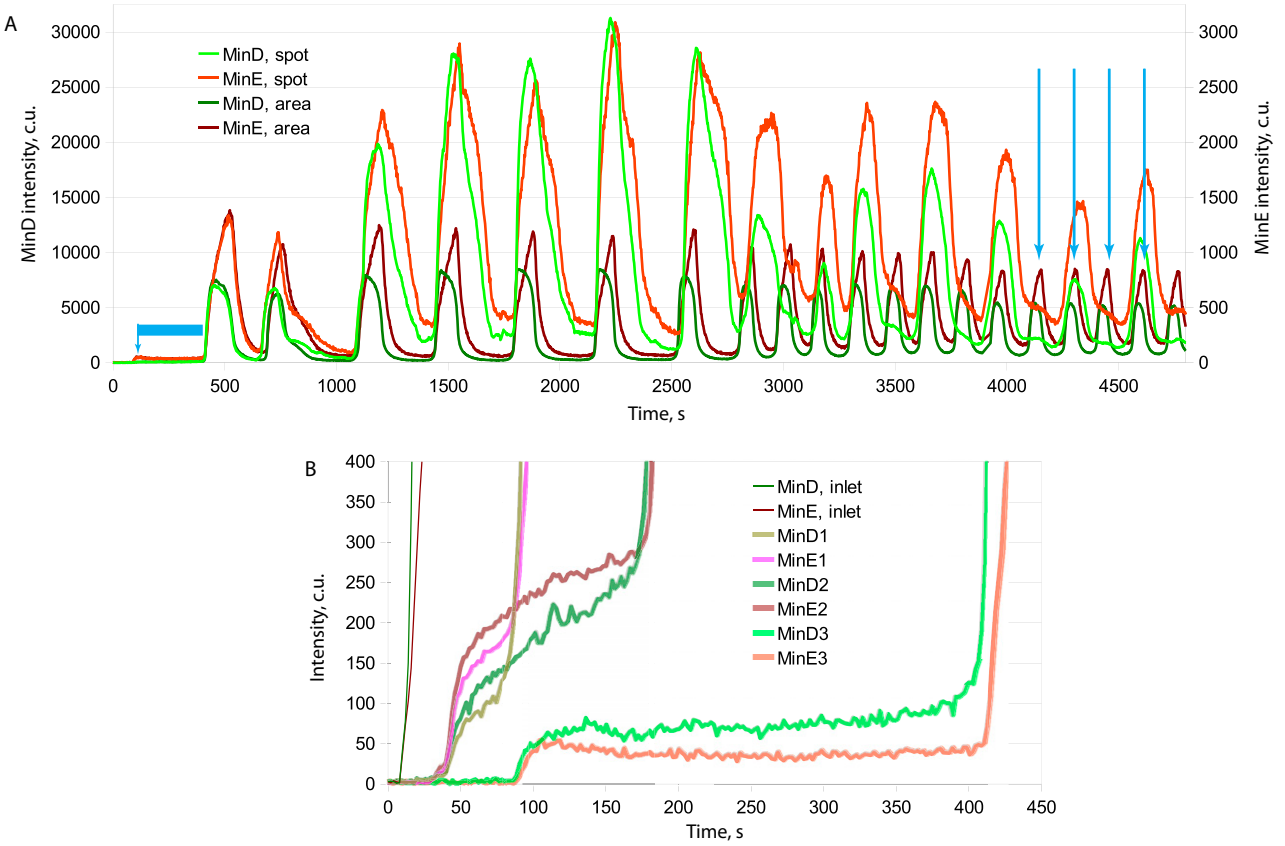

Fig. S3. (*A*) Intensity time-course for the oscillating spot within an area with propagating waves on the *E. coli* lipid bilayer shown in Movie S1. The time-course of MinD (green colors, left scale) and MinE (red colors, right scale) surface intensities is displayed with a brighter set of colors for the wave area and a darker set of colors for the oscillating spot. The last four wave periods at the time points indicated by arrows on this graph are shown in Fig. 1*C*. Several periods of oscillation switched to waves with double frequency and smaller amplitude at the approximate time 2,700 s, although the small spot continued with the frequency and amplitude of the oscillation. The graph describes MinD and MinE intensity measured at close locations in the wave and the spot areas. The fluctuations of the peak intensities for the spot are partially due to the spot motion (the brightness measurement areas were fixed). The time lag between arrival of the bulk protein and beginning of protein binding is labeled with a blue flag. (*B*) Time lag for initial binding of MinD (green) and MinE (red) near the inlet (thin line) and in the middle of the flow cell (thick shaded curve sets 1–3). In the middle of the flow cell, protein binding happens with a significant time lag between the arrival of the high concentration of proteins (coincides with the initial small step approximately 50–150 c.u.) and the rapid signal increase to a level observed in steady self-organized modes (steep portions of the curves that go off scale in this figure). The curve sets 1 and 2 were measured in one flow cell within the same field of view (Figs. S6 and S10*A*, Movie S7). The earlier rise of curve set 1 (relative to curve set 2) corresponds to a premature wave that turned into a stationary line of amoebas (presumably because the amount of initiation precursors in the solution was insufficient for steady wave propagation). The line of amoebas was later absorbed by a more standard wave arriving from the bottom with a long period described by curve set 2. The curve set 3 measured further away from the inlet was zoomed in from *A* (Movie S1).

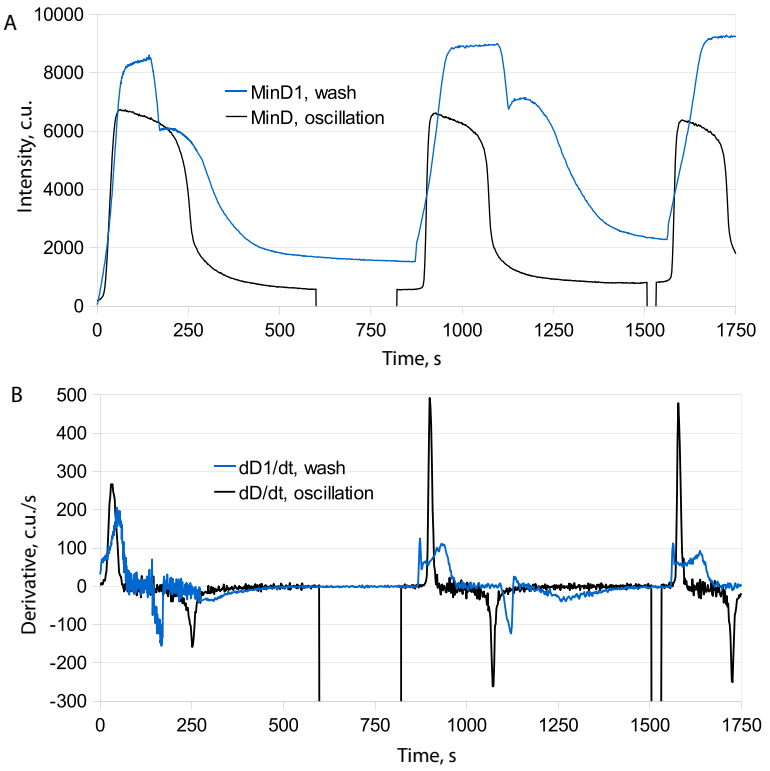

Fig. S4. Comparison of MinD binding rates during oscillation and washing cycles in presence of ATP without MinE, over *E. coli* lipid bilayers. The time axis is broken to synchronize beginning of oscillation cycles with the beginning of washing cycles. The concentration of MinD for washing cycles was 0.84 μM (less than the concentration of MinD for oscillation, 1.06 μM), but we did not detect a significantly faster MinD binding rate without MinE with higher protein concentration or with different lipid composition. (*A*) Time course of washing cycles (no MinE, same as in Fig. S2*B*) and oscillation (same as in Fig. 1*D*). (*B*) Time derivatives of surface concentrations in *A*. For the first period of oscillation the peak binding rate was slightly higher and narrower than that of the washing cycle without MinE, but the peak binding rate of oscillation became almost twice higher and twice more narrow for the second and subsequent cycles. We suggest that the faster binding transition during the second and subsequent cycles indicates production of a substantial amount of the initiation complexes upstream of the observation point.

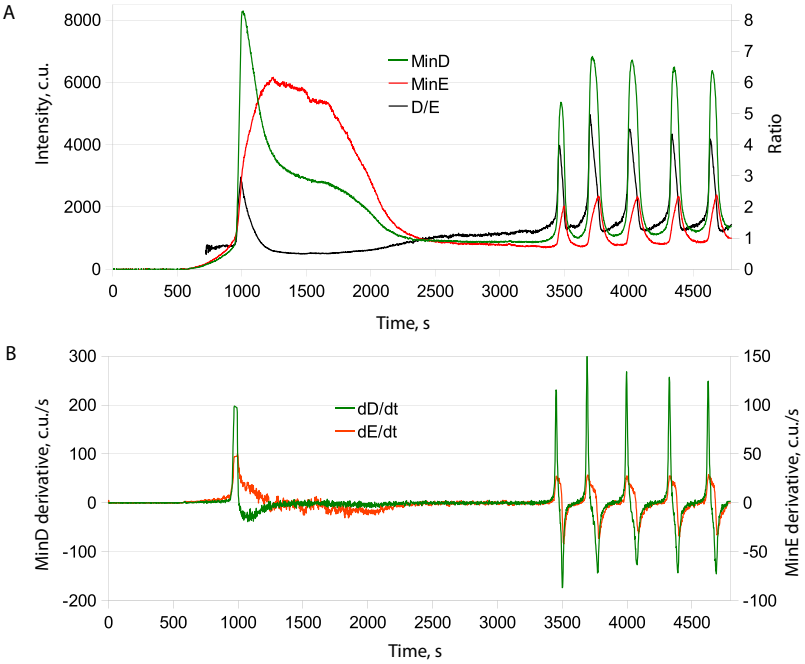

Fig. S5. (*A*) Sample introduction procedure impacts the time-course of MinD and MinE (on *E. coli* lipid bilayer) surface fluorescence intensity changes (left scale) and their ratio (right scale). The standard protein mixture was loaded into the flow cell with a gradual concentration ramp because of the Taylor dispersion in the tubings. Escape from the "steady state" of higher surface protein density required periods of higher sample flow rate. (*B*) Time derivatives of MinD (left scale) and MinE (right scale) signal intensities of *A*.

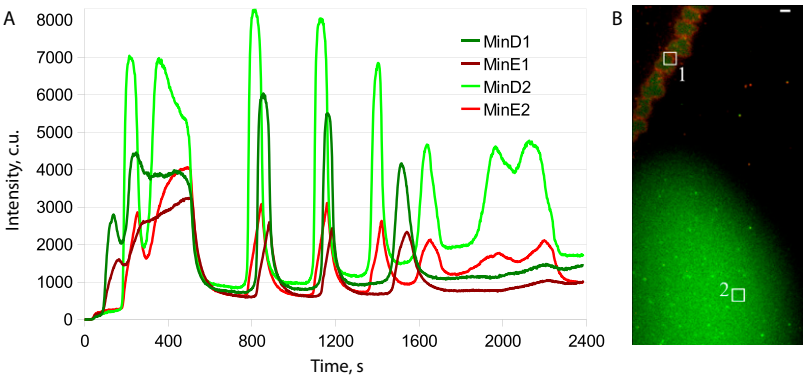

Fig. S6. (*A*) Time-coarse of MinD and MinE surface intensities for Movie S7 measured at two spots shown on the snapshot in *B* (18:2 bilayer). The first small peak for MinD #1 at time 160 s corresponds to formation of a line of amoebas. The subsequent larger peak at approximately 260 s corresponds to the maxima of oscillation. The minimum at 300 s is the time of amoeba formation. The subsequent large broad peak at approximately 400 s corresponds to formation of the continuous mesh. Two very broad high amplitude waves are passing at 860 and 1,180 s. A smaller amplitude wave arrives after 1,400 s and splits into a herd of amoebas. This process is complete by the time 1,600 s. Subsequent intensity changes reflect motion of amoebas above the intensity tracking spot. (*B*) Two spots, 3.3 × 3.3 μm each, used for intensity tracking in *A*.

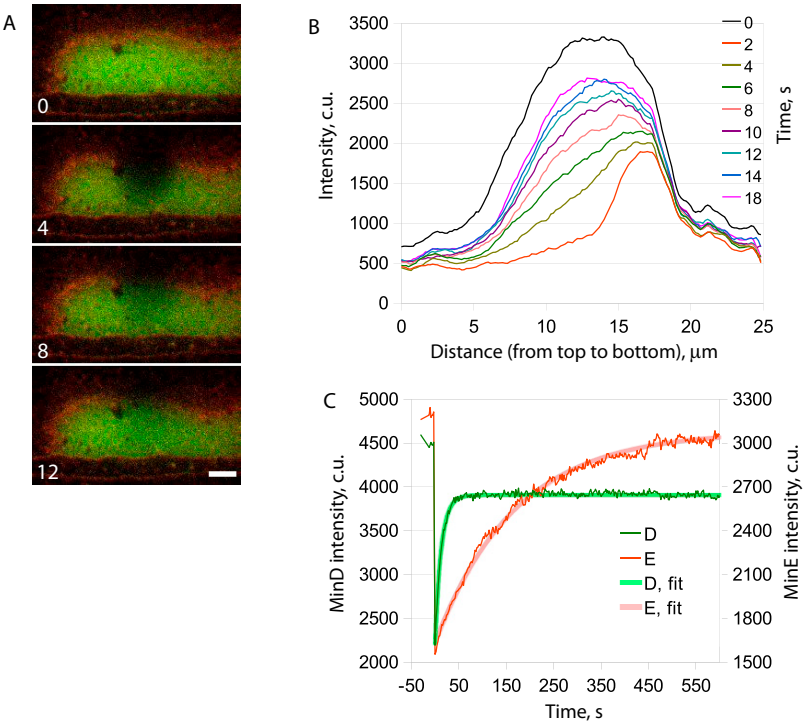

Fig. S7. Giant amoeba on *E. coli* lipid bilayer (*A*) in a FRAP experiment. The amoeba was bleached between time 0 and 2 s. The sequential frames are sorted from top to the bottom. (*B*) MinD averaged intensity profiles along a vertical line across a giant amoeba during FRAP experiment. MinD fluorescence recovery time was 6 s. (*C*) Time-course of MinD and MinE surface fluorescence intensities fitted by single exponential functions with time constants 13 and 168 s, respectively. The MinD signal is not fully recovered, although the MinE signal recovered slower, but almost to 100%.

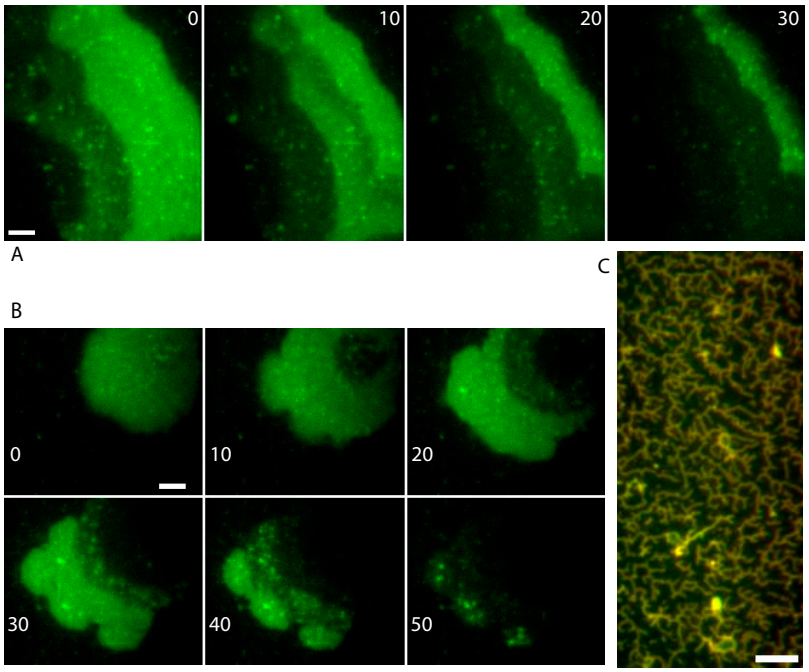

Fig. S8. Transitional states between different modes of self-organized behavior. The sequential frames are sorted from left to right in the rows going from top to the bottom. (*A*) Wave propagating in steps on *E. coli* lipid bilayer. (*B*) Mushroom-like propagation of the steps on *E. coli* lipid bilayer. The growth initiated in several distinct points on the preceding step front. (*C*) Labyrinth formed together with snake-like structures on *E. coli* lipid bilayer. The image was an average of several frames in Movie S3.

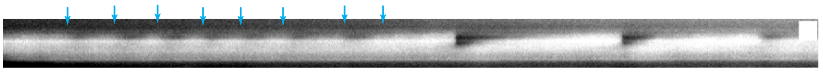

Fig. S9. Kymograph (intensity distribution) of MinD across slowly moving amoeba on the 18:2 bilayer. The time axis is horizontal from the left to the right, the spatial axis is vertical. [Scale bar: (in horizontal direction) 60 s × 5 μm (vertically).] The amoeba was periodically breathing: blue arrow shows time of the maximal expansion. Near the end of the kymograph the amoeba shrunk in steps and expanded again several times.

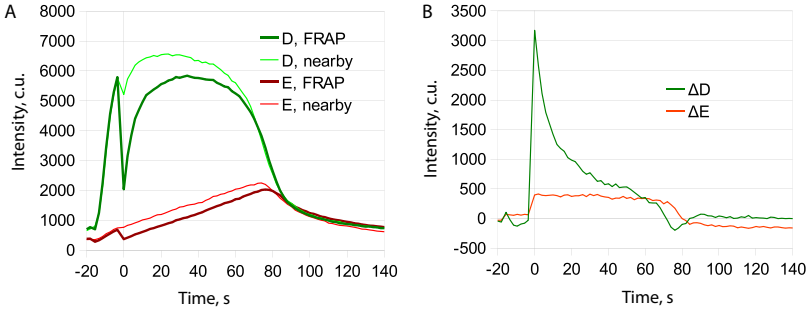

Fig. S10. Time-course of MinD and MinE surface fluorescence intensities during FRAP experiments. (*A*) Propagating wave over *E. coli* lipid bilayer was spot bleached at time 0 and the time course of MinD and MinE surface intensity was measured for the bleached spot and a spot nearby (bleached just a little). (*B*) Difference in surface intensity between unbleached and bleached spots in *A*. There was no significant recovery of MinE fluorescence. (One can notice that ΔE graph is slightly negatively sloped during time interval 0–80 s, but the baseline observed before 0 s and after 80 s is equally sloped due to small mismatch in wave amplitude and phase between two different locations used for the calculation of ΔD and ΔE.)

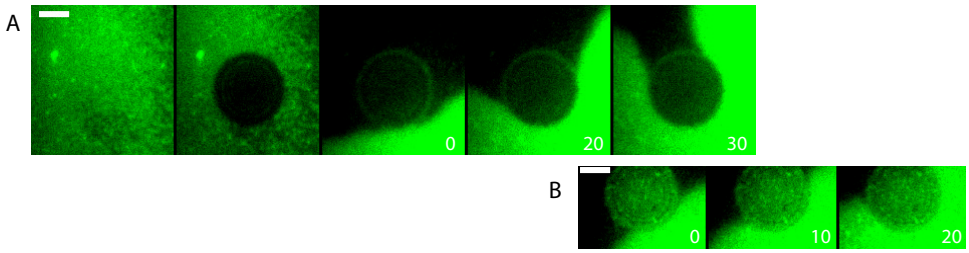

Fig. S11. Photobleaching experiments with waves propagating on *E. coli* lipid bilayer in the absence of ascorbic acid or oxygen scavenger. The sequential frames are sorted from left to right. (*A*) Photobleaching of a circular spot near the trailing edge of a wave (first two frames) leads to repulsion of the front edge of the subsequent wave from the bleached spot (last three frames). (*B*) Photobleaching of a circular spot near the front edge of a wave does not lead to strong repulsion of the front edge of the subsequent wave from the bleached spot. The wave front of the subsequent wave is straight nearby.

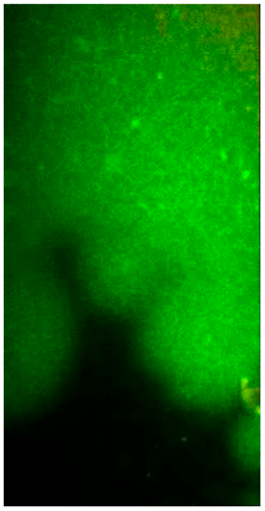

Movie S1. Oscillation and wave colocalized over *E. coli* lipid bilayer, described in Fig. 1*C* and Fig. S3*A*. The data acquisition was paused near the movie end and several frames are missing.

Movie S1

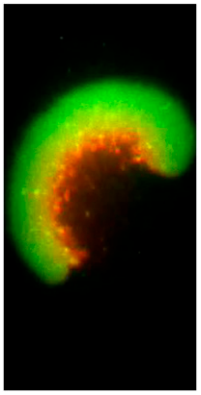

Movie S2. Waves observed after several hours of the continuous flow of the reaction mix in a flow cell coated with *E. coli* lipid bilayer after all amoeba related frozen structures got dissolved. The field of view was moved from the area with waves with straight wave fronts to an area with curved wave fronts near the end of the movie. The wave-velocity was 0.33 μm s^{-1} and period was 123 s.

Movie S2

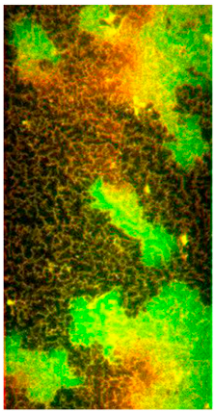

Movie S3. Waves over *E. coli* lipid bilayer propagating over the labyrinth formed by E-mesh-like structures. The same labyrinth structure is shown in Fig. S8*C*.

Movie S3

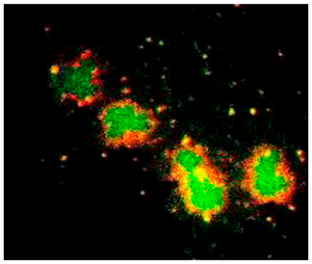

Movie S4. Slow amoebas over the 18:2 bilayer; see also Fig. 2 *C* and *D*. Some slow steady amoebas are "breathing" (slightly fluctuating in size) with a period of approximately 2 min (see kymograph in Fig. S9).

Movie S4

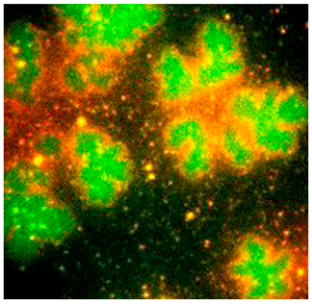

Movie S5. Movie of a group of fast traveling amoebas over the 18:2 bilayer, the same as in the Fig. 2*B*.

Movie S5

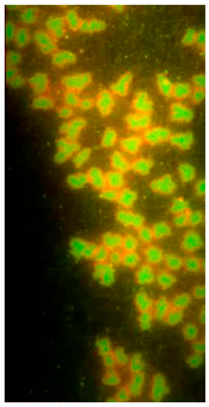

Movie S6. Wave stopped by formation of E-ring structure along the wave front splits into amoebas. The experiment was performed on the 18:1 bilayer at an elevated temperature (25 °C), compare with Fig. 2*B* and Movie S5.

Movie S6

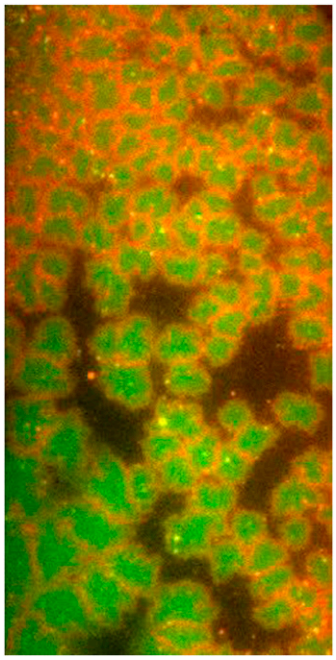

Movie S7. This movie shows waves, amoeba mesh, and amoebas over the 18:2 bilayer. Notice, that in the beginning of movie, a propagating wave stopped by forming an E-ring-like line along the wave front and developed into a line of amoebas. Figs 2*B*, 3 *A* and *B*, and Movie S5 are the parts of this movie.

Movie S7

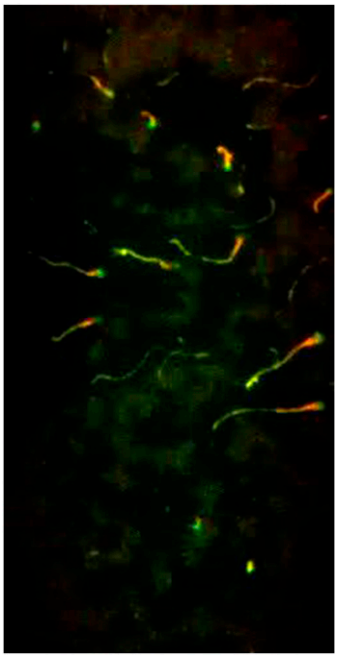

Movie S8. Snakes on the 18:1 bilayer, the same as in Fig. 4.

Movie S8

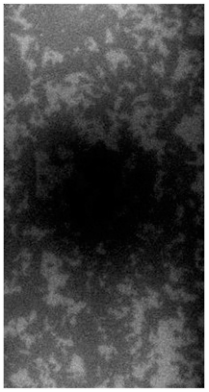

Movie S9. FRAP experiment with *E. coli* lipid bilayer stained with 2% NAO. Fast 2D diffusion of NAO (diffusion coefficient 5.7 $\mu m^2 s^{-1}$) replaces photobleached molecules in the illumination spot.

Movie S9